EFDA–JET–PR(10)59

E. Zilli, M. Brombin, A. Boboc, A. Murari
and JET EFDA contributors

On the Causes of Anomaly in the Polarimetric Measurements at JET

On the Causes of Anomaly in the Polarimetric Measurements at JET

E. Zilli[1], M. Brombin[1], A. Boboc[2], A. Murari[1]
and JET EFDA contributors*

JET-EFDA, Culham Science Centre, OX14 3DB, Abingdon, UK

[1]Consorzio RFX, Associazione EURATOM–ENEA sulla Fusione, 35127 Padova, Italy
[2]EURATOM-CCFE Fusion Association, Culham Science Centre, OX14 3DB, Abingdon, OXON, UK
** See annex of F. Romanelli et al, "Overview of JET Results",*
(23rd IAEA Fusion Energy Conference, Daejon, Republic of Korea (2010)).

Preprint of Paper to be submitted for publication in
IEEE Transactions on Plasma Science

ABSTRACT

A recent investigation of an anomaly in the polarimetric measurements at JET is reported. A calculation, based on the Stokes vector and Mueller matrix method, has been developed to simulate the effects of the waveguide on the polarization of the propagating beams. These effects consist in rotations of the polarization and alterations of the ellipticity, and affect both the probing and the reference beams. The model which is assumed here is made up of a rotated retarder followed by a rotator, with three free parameters to be optimized.

A very good agreement between the resulting calculated curves and the experimental calibration diagrams is obtained for the four vertical channels of the JET polarimeter. Variations of both phase shift and amplitude ratio are fitted by the model. This result supports the hypothesis that the waveguide system, which transfers the beams from the torus to the detectors, is the main source of the anomaly.

1. INTRODUCTION

In a previous paper [1], a detailed investigation of an anomaly in JET polarimetric measurements was carried out. This anomaly makes the interpretation of the detected signals difficult, because the direct use of the raw measurement data would lead to large errors. Thus, JET polarimetric signals are processed using a calibration code that estimates the effects of the anomaly from the calibration procedure and gives reliable measurement results [2, 3]. The presence of the anomaly is made evident during the calibration in the absence of plasma: as the polarization of the probing beam is rotated (by an angle α), the phase shift φ between the polarimetric signal and the interferometric signal is not constant, as expected, and exhibits a large variation (more than 150°, for a variation of a of 20°). The dielectric waveguides used to transfer the recombined beam from the torus hall to the detectors have been considered as a possible origin of the anomaly, which is expected to be mainly due to reflections on metal mirrors, with consequent rotations of the polarization of the beams. Simulated values of the phase shift φ as a function of α, produced by a rotation of the polarization along the waveguide, were estimated, and the calculated curves of φ versus α have been compared with the experimental calibration curves for the four vertical channels, as reported in Ref. [1].

It is observed, however, that the variations of j in the experimental curves are somewhat larger than in the curves calculated in such way. The calibration curve of Channel 3, for instance, exhibits about 170°-variation, and the simulated one about 140°. This suggests the idea that probably the rotation of the polarization is not the only effect suffered by the beams propagating along the line, but also other effects should be considered. In particular, alterations of the ellipticity are likely. Indeed, since metal mirror surfaces behave like half-wave retarders, the change of the orientation of the polarization ellipse of an incident beam should be accompanied by a reversed ellipticity [4]. Moreover, Crenn et al. [5] pointed out that a laser beam propagating along a hollow circular waveguide of the kind used at JET, may suffer some deterioration of the polarization. This may occur when the beam axis is not perfectly parallel to the guide axis, or in presence of some mechanical

defects of the guide. Components such as bends or couplers, may also produce similar effects. It should be mentioned also that the focalizing spherical mirrors, with non zero incidence angles, may produce aberrations [6], associated to changes of the polarization. So, it looks quite likely that JET waveguides, being complex systems, with many mirrors and bends, may produce both rotations of the polarization and alterations of the ellipticity of the propagating beams. For this reason, it was decided to develop a calculation based on the Mueller method, to give a more realistic simulation of the effects produced by the waveguide on the polarization of the propagating beams. The fit of the experimental measurements, obtained in JET pulses during the calibration phase before the plasma shot, has been widely investigated. The paper is organized as follows: In Section 2 a brief description of the diagnostic and a review of the basic aspects of the JET polarimeter operation are given, for a better understanding of the results presented in the following. In Section 3, the new simulation analysis for the calculation of the detector signals is presented. In Section 4, the comparison of the calculated curves with the experimental calibration curves of the four vertical channels is reported. Variations of both phase shift and amplitude ratio have been fitted with calculated curves.

2. PRELIMINARY REMARKS

The schematic of a vertical chord in the polarimeter at JET is presented in Figure 1. A reference frame is assumed with x-axis along the toroidal direction, the y-axis along the radial direction of the torus and the z-axis in the vertical direction ("Torus Coordinate System"). The probing beam coming from a DCN ($\lambda = 195\mu m$) laser passes through a half-wave plate, used for the calibration and the diagnostic set-up, before entering the vacuum vessel. The polarization is set linear at 45° with respect to the x-axis. After passing through the plasma, the polarization of the radiation experiences a rotation (Faraday effect) and acquires ellipticity (Cotton-Mouton effect).

The reference (or modulated) beam is linearly polarized at 45° and is frequency shifted of 100kHz ($\omega_0 = 2\pi \times 10^5\ sec^{-1}$) by a rotating grating wheel, before being recombined with the probing beam by a quartz plate. The two superposed beams at frequencies $\omega = 2\pi c/\lambda$ and $\omega + \omega_0$ respectively ("Recombined beam"), pass through an oversized dielectric waveguide (Pyrex tube of ~80mm inner diameter) up to a wire grid analyzer, that divides the electric field components in the x and y directions. Then these latter are focused onto two corresponding detectors ("interferometer detector" for x-component field and "polarimeter detector" for y-component field) to be acquired.

The signals from the x-component and y-component detector, indicated as i(t) ("interferometer signal") and p(t) ("polarimeter signal") respectively, are beat signals at the frequency ω_0:

$$i(t) = A_i \cos \omega_0 t \tag{2.1}$$

$$p(t) = A_p \cos(\omega_0 t - \varphi) \tag{2.2}$$

They are processed by a phase sensitive analog electronics module, to produce the

four signals:

$$RMS = \langle i(t) \cdot i(t) \rangle = \tfrac{1}{2} A_i^2 \tag{2.3}$$

$$PSD = \langle (t) \cdot \dot{p}(t) \rangle = \tfrac{1}{2} A_i A_p \cos\varphi \tag{2.4}$$

$$RMS' = \langle i'(t) \cdot i'(t) \rangle = \tfrac{1}{2} A_i'^2 \tag{2.5}$$

$$PSD' = \langle i'(t) \cdot p(t) \rangle = \tfrac{1}{2} A_i' A_p \sin\varphi \tag{2.6}$$

where $i'(t) = A_i' \sin\omega_0 t$ is generated by 90° phase shifting i(t). Then, the following ratios are calculated:

$$R = \frac{PSD}{RMS} = \frac{A_p}{A_i} \cos\varphi \tag{2.7}$$

$$R' = \frac{PSD'}{\sqrt{RMS \cdot RMS'}} = \frac{A_p}{A_i} \sin\varphi, \tag{2.8}$$

from which the next equations are readily obtained:

$$\frac{A_p}{A_i} = \sqrt{R^2 + R'^2} \tag{2.9}$$

$$\varphi = \arctan\left(\frac{R'}{R}\right). \tag{2.10}$$

In ideal conditions, these two quantities are directly related to the angles which define the polarization state of the radiation exiting the plasma

$$\Theta = \arctan\left(C \frac{A_p}{A_i}\right) \tag{2.11}$$

$$\Phi = \varphi - \phi_0 \tag{2.12}$$

C and ϕ_0 being calibration constants [1]. In particular, using (2.11) and (2.12), the Faraday rotation angle and the ellipticity due to the Cotton-Mouton effect are readily deduced. As a consequence of the anomaly, however, this procedure would give wrong results, if the raw measurement data are used directly. For this reason, at JET, the polarimetric signals are processed using a suitable calibration code [2,3].

3. ANALYSIS OF THE SIMULATION

As shown in Ref. [1], the probing beam, propagating in the z-direction with amplitude E_0, after passing through the plasma and the recombination plate, can be expressed as

$$E_x^{(p)} = |P_\perp| e^{i\psi_\perp} \cdot E_0 \cos\Theta \tag{3.1}$$

$$E_y^{(p)} = |P_{//}| e^{i\psi_{//}} \cdot E_0 \sin\Theta e^{-i\Phi}, \tag{3.2}$$

with time dependence e^{-iwt}, $\omega = 2\pi c/\lambda$, and

$$\Theta = \Theta_0 + \alpha \tag{3.3}$$

with $\Theta_0 = 45°$. In the absence of plasma, α is produced by a rotation of the half-wave plate used for the calibration. It is twice the rotation angle of the plate. In the presence of plasma, a is due to the Faraday effect, and Φ is the phase shift between the x and y electric field components due to the Cotton-Mouton effect.

Similarly, the reference beam of amplitude E_{0g}, after being reflected by the recombination plate, can be expressed as:

$$E_x^{(r)} = |R_\perp| e^{i\phi_\perp} \cdot \frac{E_{0g}}{\sqrt{2}} \tag{3.4}$$

$$E_y^{(r)} = |R_{//}| e^{i\phi_{//}} \cdot \frac{E_{0g}}{\sqrt{2}}, \tag{3.5}$$

with time dependence $e^{-i(\omega + \omega_0)t}$. The numerical values of the parameters associated to the recombination plate, calculated in Ref. [1], are reported in Table 1.

Up to this point, the Jones formalism has been adopted, because it is very well suited for describing the effects of the quartz recombining plate on the beams. However, it is thought useful to switch to the Stokes vector and Mueller matrix formalism to describe better the changes of polarization of the propagating beams in the waveguide. For the probing beam, the following two angles are evaluated:

$$\Theta_i^{(p)} = \arctan\left(\frac{|P_{//}|}{|P_\perp|}\tan\Theta\right), \qquad 0 \le \Theta_i^{(p)} \le \frac{\pi}{2} \tag{3.6}$$

$$\Phi_i^{(p)} = \psi_\perp - \psi_{//} + \Phi, \qquad (-\pi \le \Phi_i^{(p)} \le \pi) \tag{3.7}$$

The amplitude ratio is given by the following formula:

$$s_{1i}^{(p)} = \cos 2\Theta_i^{(p)} \tag{3.8}$$

$$s_{2i}^{(p)} = \sin 2\Theta_i^{(p)} \cdot \cos\Phi_i^{(p)} \tag{3.9}$$

$$s_{3i}^{(p)} = \sin 2\Theta_i^{(p)} \cdot \sin\Phi_i^{(p)}. \tag{3.10}$$

Similar calculations for the reference beam are as follows:

$$\Theta_i^{(r)} = \arctan \frac{|R_{//}|}{|R_{\perp}|} \qquad 0 \le \Theta_i^{(r)} \le \frac{\pi}{2} \tag{3.11}$$

$$\Phi_i^{(r)} = \phi_{\perp} - \phi_{//} \qquad (-\pi \le \Phi_i^{(r)} \le \pi) \tag{3.12}$$

$$s_{1i}^{(r)} = \cos 2\Theta_i^{(r)} \tag{3.13}$$

$$s_{2i}^{(r)} = \sin 2\Theta_i^{(r)} \cdot \cos \Phi_i^{(r)} \tag{3.14}$$

$$s_{3i}^{(r)} = \sin 2\Theta_i^{(r)} \cdot \sin \Phi_i^{(r)}. \tag{3.15}$$

Neglecting the attenuation in the waveguide, the intensities of both the probing and reference beams are constant during the propagation

$$I^{(p)} = E_0^2 \cdot \left(|P_{\perp}|^2 \cos^2 \Theta + |P_{//}|^2 \sin^2 \Theta \right) \tag{3.16}$$

$$I^{(r)} = \tfrac{1}{2} E_{0g}^2 \cdot \left(|R_{\perp}|^2 + |R_{//}|^2 \right). \tag{3.17}$$

Since the reduced 3-component Stokes vector can be used in place of the full 4-component Stokes vector, this allows to use (3×3) sub-matrices instead of complete (4×4) Mueller matrices.

If **M** is the transformation matrix which describes the changes produced by the waveguide in the beam polarization, then the final Stokes vectors of the two beams can be respectively obtained by

$$\mathbf{s}_f^{(p,r)} = \mathbf{M} \cdot \mathbf{s}_i^{(p,r)}. \tag{3.18}$$

In the hypothesis of an ideal grid, the beat signals at the detectors are given by

$$i(t) = K_x \left(E_x'^{(p)} E_x'^{(r)*} e^{i\omega_0 t} + c.c. \right) \tag{3.19}$$

$$p(t) = K_y \left(E_y'^{(p)} E_y'^{(r)*} e^{i\omega_0 t} + c.c. \right), \tag{3.20}$$

where K_x and K_y are proportional to the respective responsivities, and hence the knowledge of the final electric field amplitudes is necessary. This can be bypassed going back to the Jones notations. To do this, the following parameters are calculated

$$\Theta_f^{(p)} = \tfrac{1}{2} \arccos s_{1f}^{(p)} \qquad \left(0 \le \Theta_f^{(p)} \le \tfrac{\pi}{2} \right) \tag{3.21}$$

$$\Theta_f^{(r)} = \tfrac{1}{2} \arccos s_{1f}^{(r)} \qquad \left(0 \le \Theta_f^{(r)} \le \tfrac{\pi}{2} \right) \tag{3.22}$$

$$\tan\Phi_f^{(p)} = \frac{s_{3f}^{(p)}}{s_{2f}^{(p)}} \tag{3.23}$$

$$\tan\Phi_f^{(r)} = \frac{s_{3f}^{(r)}}{s_{2f}^{(r)}} \tag{3.24}$$

$$E_x'^{(p)} = \sqrt{I^{(p)}}\cos\Theta_f^{(p)} \tag{3.25}$$

$$E_y'^{(p)} = \sqrt{I^{(p)}}\sin\Theta_f^{(p)} e^{-i\Phi_f^{(p)}} \tag{3.26}$$

$$E_x'^{(r)} = \sqrt{I^{(r)}}\cos\Theta_f^{(r)} \tag{3.27}$$

$$E_y'^{(r)} = \sqrt{I^{(r)}}\sin\Theta_f^{(r)} e^{-i\Phi_f^{(r)}} \tag{3.28}$$

Then, by using the Equations (3.19) and (3.20), it is possible to express the detector signals in the form (2.1) and (2.2), with

$$A_i = 2K_x\sqrt{I^{(p)}I^{(r)}}\cos\Theta_f^{(p)}\cos\Theta_f^{(r)} \tag{3.29}$$

$$A_p = 2K_y\sqrt{I^{(p)}I^{(r)}}\sin\Theta_f^{(p)}\sin\Theta_f^{(r)} \tag{3.30}$$

$$\varphi = \Phi_f^{(p)} - \Phi_f^{(r)} \tag{3.31}$$

Furthermore, from (3.23) and (3.24) the phase shift φ and tanφ may be expressed as

$$\tan\varphi = \tan\left(\Phi_f^{(p)} - \Phi_f^{(r)}\right) = \frac{\tan\Phi_f^{(p)} - \tan\Phi_f^{(r)}}{1 + \tan\Phi_f^{(p)}\tan\Phi_f^{(r)}} \tag{3.32}$$

$$\varphi = \arctan\frac{\tan\Phi_f^{(p)} - \tan\Phi_f^{(r)}}{1 + \tan\Phi_f^{(p)}\tan\Phi_f^{(r)}} \tag{3.33}$$

The amplitude ratio is given by the following formula:

$$\frac{A_p}{A_i} = \frac{K_y}{K_x}\tan\Theta_f^{(p)}\tan\Theta_f^{(r)}. \tag{3.34}$$

The transformation matrix, which is introduced here to simulate the effects of the waveguide, is the product of two matrices

$$\mathbf{M} = \mathbf{M}_R(\theta)\cdot\mathbf{M}_C(\Delta,\gamma) \tag{3.35}$$

the former is the matrix for a rotation of an angle θ, with unchanged ellipticity

$$\mathbf{M}_R(\theta) = \begin{pmatrix} \cos 2\theta & \sin 2\theta & 0 \\ -\sin 2\theta & \cos 2\theta & 0 \\ 0 & 0 & 1 \end{pmatrix} \tag{3.36}$$

the latter is the matrix for a rotated retarder, having a relative retardation D and its principal axis at an angle γ to the x direction

$$\mathbf{M}_C(\Delta,\gamma)=\begin{pmatrix}\cos^2 2\gamma+\cos\Delta\sin^2 2\gamma & (1-\cos\Delta)\sin 2\gamma\cos 2\gamma & -\sin\Delta\sin 2\gamma\\ (1-\cos\Delta)\sin 2\gamma\cos 2\gamma & \sin^2 2\gamma+\cos\Delta\cos^2 2\gamma & \sin\Delta\cos 2\gamma\\ \sin\Delta\sin 2\gamma & -\sin\Delta\cos 2\gamma & \cos\Delta\end{pmatrix} \tag{3.37}$$

When

$$\Delta=\pi+\delta, \tag{3.38}$$

δ being a small angle, the retarder behaves like a non ideal half-wave plate, whichproduces a rotation associated with a change of the ellipticity. In the product (3.35) the two matrices are ordered such that a propagating beam encounters first the retarder and then the rotator. It may be expected that the retarder gives a good representation of the effect of the metal mirrors. Nevertheless, rotations with unchanged ellipticity might also be possible. As an example, the orientation of the analyzing wire grid in front of the detectors defines "The Local Coordinate System of the Grid", which may be different from the "Torus reference frame" x, y, z [2]. This could have the effect of rotating the polarization of the beam.

4. RESULTS OF THE SIMULATIONS

The simulation analysis described in Section III has been used to find the best fit of various plots of the phase shift φ and of the amplitude ratio A_p/A_i versus α, obtained in the calibration phase, before JET pulses. The experimental curves are calculated using the acquired data of R and R', using Eqs. (2.9) and (2.10). The four vertical channels of the Pulse No's: 74650 (September 11, 2008) and 79692 (October 16, 2009) are considered in this work.

First of all, it should be noted that both the experimental and the theoretical data of are given as solutions of the arctan function, defined by Eqs. (2.10) and (3.33), respectively. As a consequence, there is an indetermination of ±π (or integer multiples of it) on the values of φ. The use of solutions limited to the interval −π/2 to +π/2, as they are usually given by computers, gives unrealistic p-jumps in diagrams. In order to avoid this, whenever it is necessary, the result is corrected by adding or subtracting π, in order to preserve the continuity of the curve, as it is natural. Moreover, the variations of φ with respect to its initial value ϕ_0 at α = 0

$$\Delta\varphi=\varphi-\phi_0 \tag{4.1}$$

are plotted as a function of a both in calculated and experimental diagrams, as it is shown in Figures 2 to 9 (top). In the same figures (bottom), the calculated and experimental diagrams of CA_p/A_i as a function of a are also shown. The amplitude ratio is multiplied by the normalizing factor $C = 1/(A_p/A_i)_{\alpha=0}$, so that their product is equal to 1 when Θ = 45°, in accordance with Eq. (2.11). The theoretical curves are calculated with Φ = 0, using the angles γ, δ and θ as adjustable parameters. The compared diagrams for the vertical channels 1, 2, 3 and 4 of the Pulse No: 74650 are shown

in Figs. 2, 3, 4, and 5, respectively; the diagrams for the same channels of the Pulse No: 79692 are depicted in Figures 6, 7, 8 and 9, respectively.

As it is clearly shown in the examples reported, the model reproduces very well the experimental curves of both the phase shift difference and of the normalized amplitude ratio, if the values of the parameters are carefully chosen. For this preliminary investigation, the search of the optimum values of the parameters has been done manually, without the need of too many attempts. Very likely, this optimization should not demand very large computation resources if it would be run automatically, before each JET pulse.

Usually, whenever a good agreement for the phase shift profile is found, an equally good agreement is automatically found for the amplitude ratio also. In particular, in the case of channel 3, the fit achieved in either phase shift and amplitude ratio diagrams has been very satisfactory for the two shots (see Figs. 4 and 8). Some discrepancies are observed, however, in the amplitude ratio curves of channel 2 in both shots, despite the good agreement of the phase shift curves (see Figures 3 and 7). The differences observed in the experimental profiles of the two shots (and consequently in the choice of the three adjustable parameters) have to be ascribed to many changes which have been performed in the diagnostic configuration in the time elapsed between the two shots. Relatively small values for δ-angle (associated with changes of ellipticity) are found, in comparison with γ and θ (both associated with rotations). This proves that the rotation of the polarization is the main effect, but a certain change of the ellipticity, though modest, is essential for a complete agreement. The differences between the experimental and theoretical initial values ϕ_0 of the phase shift φ, have no physical relevance. The experimental value of ϕ_0 in fact depends on the instrumental setup. Anyway, ϕ_0 is not significant in polarimetric measurements, since the Cotton-Mouton effect is related to the difference $j - \phi_0$ and not to the absolute value of φ, whereas the Faraday effect to the amplitude ratio A_p/A_i, independent on φ.

At JET, before each campaign, or when it is necessary, a manual calibration is performed, which consists of the fine tuning of the wire grid position, located in front of the two detectors. This allows modifying the repartition of the signal between the interferometric and the polarimetric detectors and therefore permits to optimise the setup of the diagnostic for the requirements of the physical programme (depending for example on the relative importance to be accorded to the interferometric and polarimetric signals). This is the case of the Pulse No: 79692, which belongs to a high plasma current campaign, where the wire grids have been rotated.

The extension of the simulation analysis to the case of arbitrary transmission and reflection coefficients proved to be unnecessary. Let be T_{gx} the (power) transmission coefficient of the grid for x-directed electric fields, and R_{gy} the reflection coefficient for y-directed fields. Best results have been achieved for T_{gx} and R_{gy} both equal to 1, and optimizing the parameters γ, δ and θ, as it was done before. This means that a wire grid, even if it is rotated, keep its "ideal" characteristics, and the effect of its rotation is equivalent to rotate the polarization of the beam impinging on it. This rotation is included in the θ-angle. This angle, as it is known, takes into account also other possible rotations of the polarization with unchanged ellipticity, as for instance the rotation of the "local" reference frame

with respect to the "Torus" reference frame. So, the best fit procedure is again performed limiting to three the number of the parameters to be optimized, without the use of additional variables.

CONCLUSIONS

The curves calculated by the model described in this paper, fit very well and simultaneously the experimental calibration curves of both the phase shift difference and of the normalized amplitude ratio, on the four vertical channels of the JET polarimeter. The data of the Pulse No's: 74650 and 79692 have been considered in this analysis. The search of the optimum values of the three adjustable parameters has been rather easy to do.

The very good agreement which is found, indicates that the rotation of the polarization is not the only cause of the anomaly. In fact, for a complete agreement, a change of the ellipticity must also be considered.

For both shots, the results are consistent with the assumption of "ideal" wire grids. If a grid has been rotated during manual calibration, as in the case of Pulse No: 79692, the model has the capability of self-adjusting to this effect, without the need of additional parameters.

These results support the hypothesis that the anomaly is mainly due to the waveguide systems, which transfer the radiation from the torus to the detectors. They produce changes in the polarization of the propagating beams (rotations and ellipticity alterations), and affect both the probing and the reference beams.

Very decisive elements to state if this hypothesis is true or not, could be given by an experimental measurement of the Mueller matrix of the waveguides. So, it would be very interesting to compare the experimentally determined matrices to the ones considered in our calculations. Methods for measuring the Mueller matrices on optical components are described in Ref. [4, 7, 8]. An example of measurement of Mueller matrix in the FIR domain is given in Ref. [9].

REFERENCES

[1]. E. Zilli, M. Brombin, A. Boboc, L. Giudicotti, A. Murari, and JET-EFDA Contributors, "Investigation on an Anomalous Behaviour of the Polarimetric Measurements at JET", IEEE Transactions on Plasma Science, Vol. PS-**38**, no. 11, pp. 3201-3210, Nov. 2010.

[2]. K. Guenther, and JET-EFDA Contributors, "'Complete' far-infrared polarimetry measurements at JET", in Proc. 31st EPS Conf. Plasma Phys., London, U.K., 28th June to 2nd July 2004, P5-172

[3]. M. Gelfusa, A. Murari, P. Gaudio, A. Boboc, M. Brombin, F. P. Orsitto, E. Giovannozzi, and JET-EFDA Contributors, "A new calibration code for the JET polarimeter", Review of Scientific Instruments, Vol. **81**, p. 053507, 2010.

[4]. D. Goldstein, Polarized Light. Marcel Dekker, Inc., New York, 2003.

[5]. J.P. Crenn, "A Study of Waveguides for Far Infrared Interferometers Measuring Electron Density of Tokamak Plasmas", IEEE Trans. Microwave Theory Technology, Vol. MTT-**27**, no. 6, pp. 573-577, Apr. 1979.

[6]. M. Born and E. Wolf, Principles of Optics. Oxford, U.K.: Pergamon, 1980.

[7]. C. Brosseau, Fundamentals of Polarized Light. John Wiley & Sons, Inc., N.Y.. 1998.

[8]. B.J. Howell, "Measurement of the polarization effects of an instrument using partially polarized light", Applied Optics, Vol. 1**8**, no. 6, p. 809-812, March 1979.

[9]. L. Giudicotti and M. Brombin, "Data analysis for a rotating quarter-wave, farinfrared Stokes polarimeter", Applied Optics, Vol. **46**, no. 14, p. 2638-2648, May 2007.

$\|P_\perp\|$	=	0.6798
$\|P_{//}\|$	=	0.9495
$\|R_\perp\|$	=	0.7334
$\|R_{//}\|$	=	0.3139
$\psi_\perp$	=	−9.6309°
$\psi_{//}$	=	−2.9590°
$\phi_\perp$	=	19.0239°
$\phi_{//}$	=	43.4187°

Table 1: Moduli and Phases of the transmission and reflection coefficients of the recombination plate.

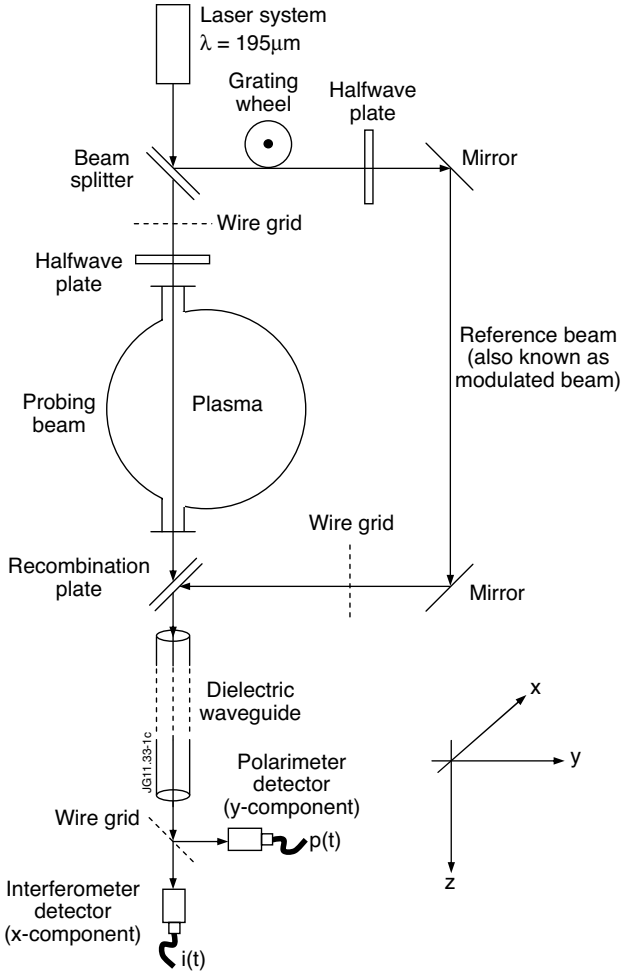

Figure 1: Diagnostic layout for one vertical chord of the interferometer/polarimeter at JET.

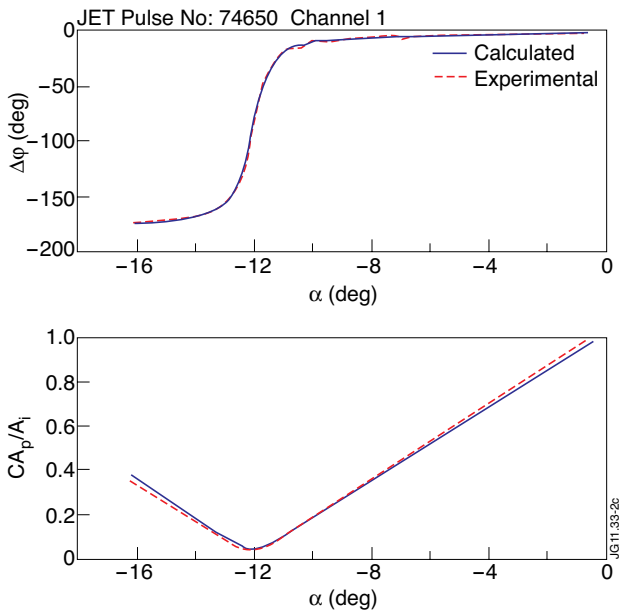

Figure 2: Comparison of experimental and theoretical curves for channel 1in 74650 JET pulse: Δφ versus α (top), and CA_p/A_i versus α (bottom), calculated with γ = 16.6°, δ = −7.4°, θ = −9.1°.

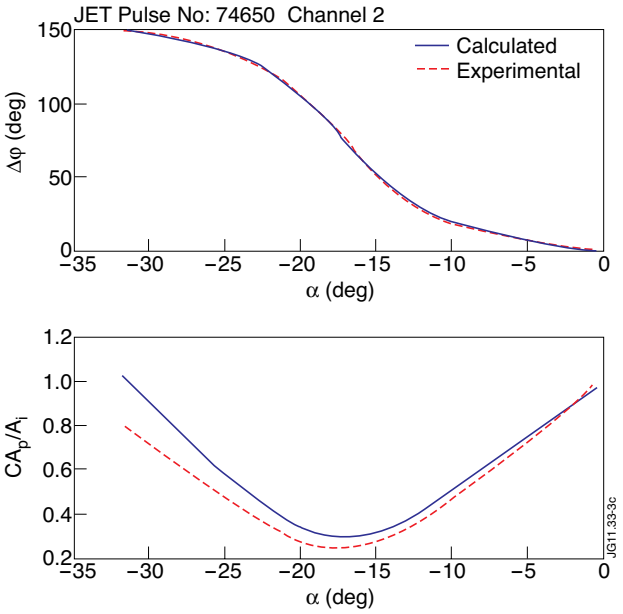

Figure 3: Comparison of experimental and theoretical curves for channel 2 in 74650 JET pulse: Δφ versus α (top), and CA_p/A_i versus α (bottom), calculated with γ = 59.5°, δ = -7°, θ = 82.4°.

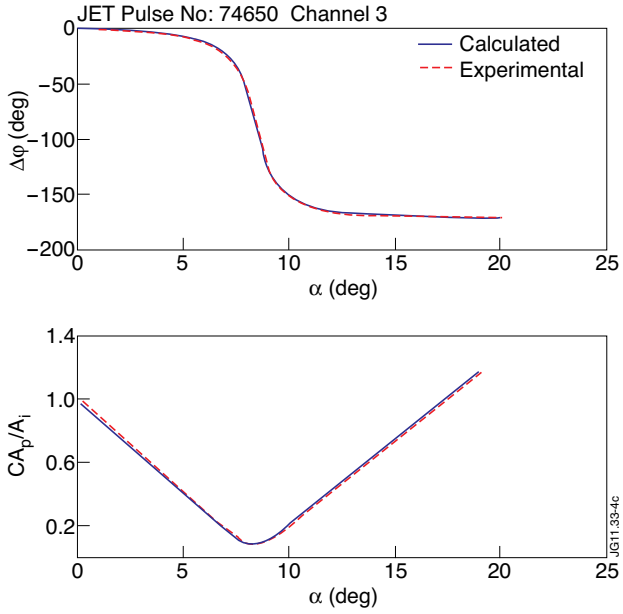

Figure 4: Comparison of experimental and theoretical curves for channel 3 in 74650 JET pulse: Δφ versus α (top), and CA_p/A_i versus α (bottom), calculated with γ = 74.5°, δ = 10°, θ = 87.15°.

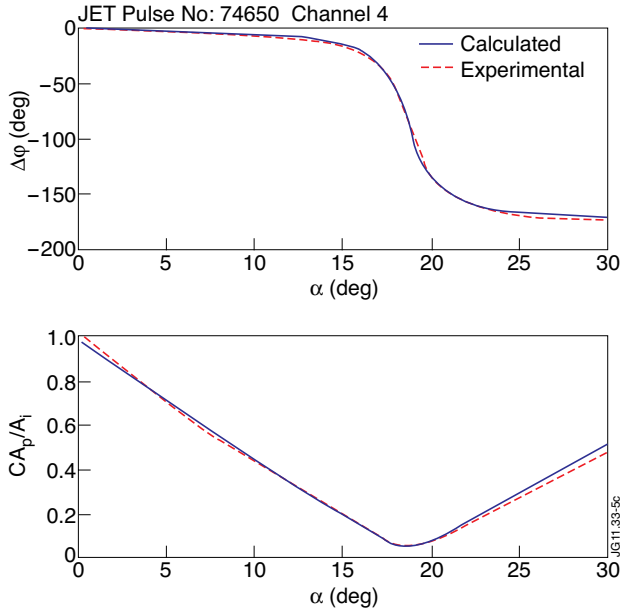

Figure 5: Comparison of experimental and theoretical curves for channel 4 in 74650 JET pulse: Δφ versus α (top), and CA_p/A_i versus α (bottom), calculated with γ = 75.2°, δ = 14°, θ = 80°.

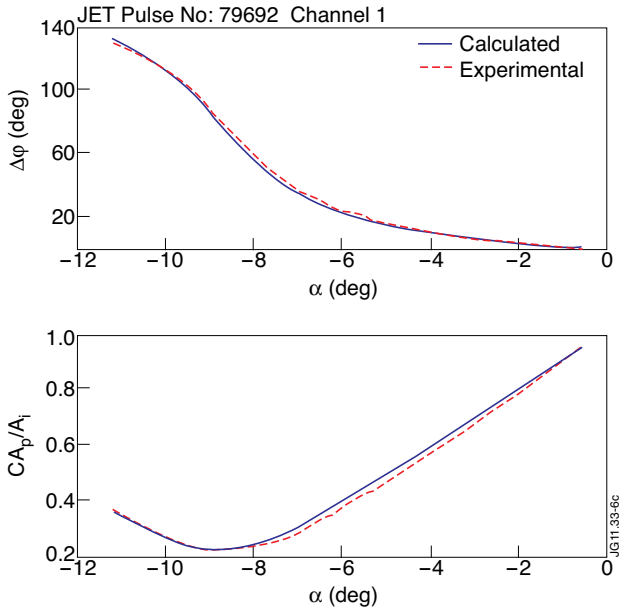

Figure 6: Comparison of experimental and theoretical curves for channel 1 in 79692 JET pulse: Δφ versus α (top), and CA_p/A_i versus α (bottom), calculated with γ = 64.6°, δ = 4.5°, θ = 83.5°.

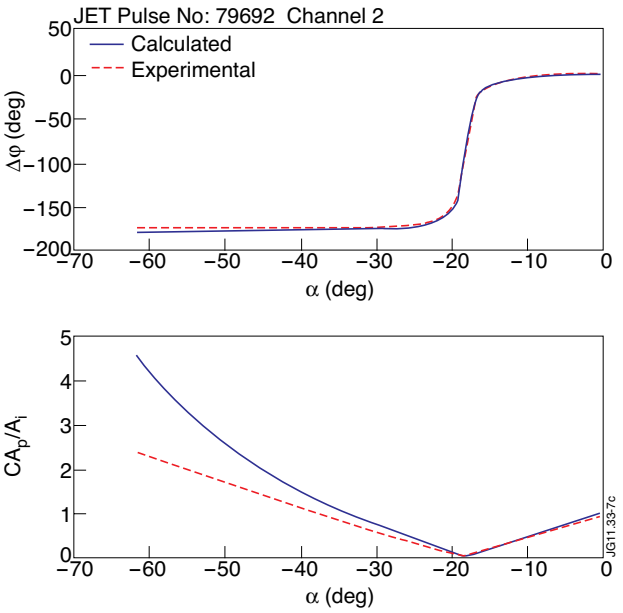

Figure 7: Comparison of experimental and theoretical curves for channel 2 in 79692 JET pulse: Δφ versus α (top), and CA_p/A_i versus α (bottom), calculated with γ = 58.8°, δ = 6°, θ = 82.5°.

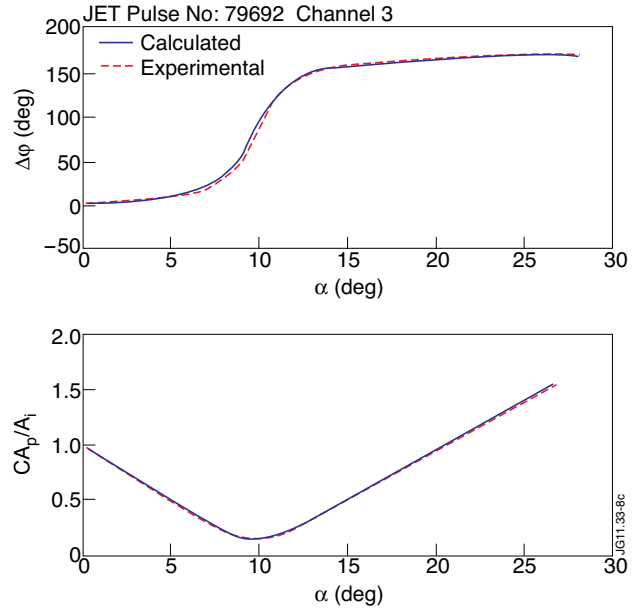

Figure 8: Comparison of experimental and theoretical curves for channel 3 in 79692 JET pulse: Δφ versus α (top), and CA_p/A_i versus α (bottom), calculated with γ = 30.1°, δ = -3.1°, θ = -3.05°.

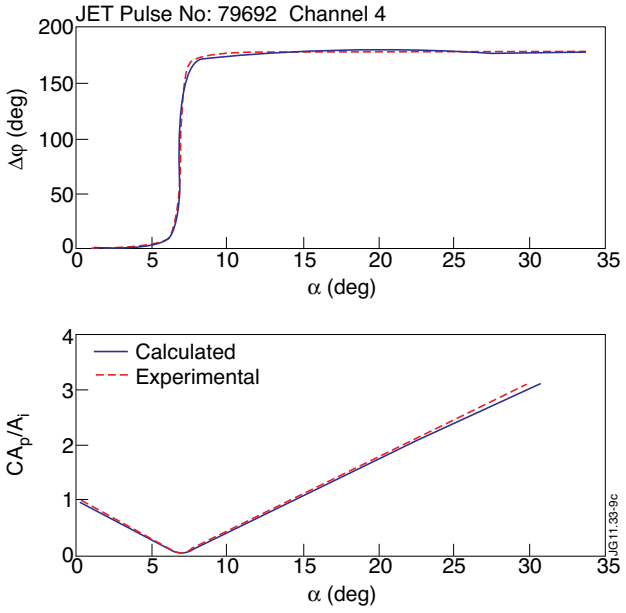

Figure 9: Comparison of experimental and theoretical curves for channel 4 in 79692 JET pulse: Δφ versus α (top), and CA_p/A_i versus α (bottom), calculated with γ = 70.2°, δ = 16.3°, θ = 80°.